

Latitudinal Distribution of Gaseous Elemental Mercury in Tropical Western Pacific: The Role of the Doldrums and the ITCZ

Fange Yue, Zhouqing Xie,* Yanxu Zhang, Jinpei Yan, and Shuhui Zhao



Cite This: *Environ. Sci. Technol.* 2022, 56, 2968–2976



Read Online

ACCESS |



Metrics & More



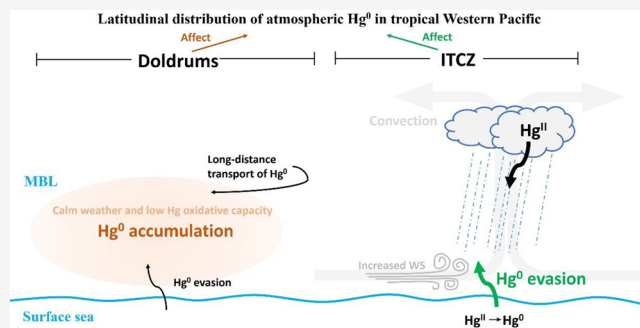
Article Recommendations



Supporting Information

ABSTRACT: The role of the tropical western Pacific in the latitudinal distribution of atmospheric mercury is still unclear. In this study, we conducted continuous measurements of gaseous elemental mercury (GEM) in the marine boundary layer (MBL) along a large latitudinal transect ($\sim 60^\circ$ S to $\sim 30^\circ$ N) of the western Pacific, accompanied by measurements of dissolved gaseous mercury (DGM) in the surface seawater. We found that the GEM latitudinal gradient is the most significant in the tropical western Pacific, which to some extent might be attributed to the impact of the doldrums and the Intertropical Convergence Zone (ITCZ) in this area. For the doldrums, calm weather may delay the transport of GEM, facilitating its accumulation in the tropical western Pacific. Furthermore, the regional transport, and low O_3 and sea-salt aerosol levels in this area which would not favor the oxidation of GEM in the MBL, would intensify the accumulation of GEM in the tropical western Pacific. For the ITCZ, the vast wet deposition of Hg would drive elevated DGM in the surface seawater, which can increase the evasion flux and may further influence the spatial distribution of GEM. This study provides insight into the role of the tropical western Pacific in the regional atmospheric mercury cycle.

KEYWORDS: mercury, doldrums, ITCZ, air-sea exchange, spatial distribution



1. INTRODUCTION

Air-sea exchange of mercury (Hg) is critical for its global cycle.^{1,2} Atmospheric deposition is the main pathway by which Hg enters the ocean.^{3,4} After being deposited to the ocean, a part of Hg can be transferred to methylated forms via abiotic and biotic reactions, thereby bioaccumulating in the marine food chain.⁵ However, most of the Hg (>80%) would emit back to the marine boundary layer (MBL) after being reduced to the dissolved gaseous mercury (DGM, mainly in the form of Hg^0).⁶ Therefore, the surface ocean seems to be a temporary reservoir for Hg. Previous studies in various oceanic regions have shown that the ocean has a strong tendency of (re)-emitting gaseous elemental mercury (GEM) to the troposphere as most sea surface waters are supersaturated with Hg^0 .^{1,7–20} Additionally, the ocean evasion of Hg to the atmosphere was estimated to be similar to that from anthropogenic emissions.^{1,21} The GEM (or Hg^0) that is subject to re-emission from the surface ocean is not only the main source of Hg in the atmosphere but also helps its long-range transmission, and this transport mechanism is also called as “grasshopper-jump”.²²

Tropical oceanic areas have a special influence on the Hg cycle in the MBL. Owing to the existence of the Intertropical Convergence Zone (ITCZ, mainly concentrated in the range of 10° S \sim 10° N), high temperature and humidity accompanied

by air convection favor the formation of precipitation in this area. Several previous studies have found strong DGM enrichment in surface waters near the equator,^{8,10,13} which was attributed to the enhanced wet deposition of atmospheric Hg and the shallow oceanic mixing layer in this area. Additionally, a recent modeling study suggested that high DGM concentrations in the ITCZ are also associated with elevated convective cloud mass flux and bromine (Br) content in the tropical upper troposphere.²³ However, its feedback and effects on the spatial distribution of atmospheric GEM require further investigation. In addition, due to the relatively small horizontal temperature and pressure gradients, some equatorial oceanic regions are characterized by persistently weak wind speeds (called the doldrums, which is usually appeared in the range of 5° near the equator),²⁴ while their potential impacts on the transport and transformation of atmospheric components (such as Hg) are still unclear.

Received: October 23, 2021

Revised: January 6, 2022

Accepted: January 31, 2022

Published: February 10, 2022



The hemispheric gradient of Hg over the Atlantic and Pacific oceans has been reported in some studies, with higher concentrations found in the northern hemisphere,^{13,25–33} which was usually interpreted as direct evidence that gaseous mercury could be transported globally (from the north, with more anthropogenic emissions, to the south). However, a sensitivity analysis of the model showed that the southern hemisphere atmospheric Hg mainly originates from oceanic emission rather than transport from the northern hemisphere.³⁴ As the border area between the northern and southern hemispheres, the role of the tropical western Pacific in the regional transport and hemispheric gradient of Hg requires further research.

As part of the 34th (2017–2018) Chinese National Antarctic Research Expedition (CHINARE) aboard the R/V Xuelong, we conducted continuous measurements of GEM in the MBL along a large latitudinal transect (~60° S to ~30° N) of western Pacific, along with corresponding observations of DGM, to better understand the cycling of Hg in the equatorial oceanic areas.

2. METHODS

2.1. Site Locations. As the returning voyage of the 34th CHINARE, the observation cruise in this study was mainly located on the western side of the Pacific Ocean, crossing the equator from the high latitude area of the Southern Ocean to the midlatitude area of the northwest Pacific, spanning a large latitudinal range (Figure S1 of the Supporting Information, SI). The latitude ranged from approximately 60° S to 30° N, and the longitude ranged from approximately 177° W to 123° E.

2.2. Experimental Methods. GEM was automatically measured using a Tekran 2537B cold vapor atomic fluorescence spectroscopic (CVAFS) Hg analyzer. Details about the method are described in Yu et al. (2014)³⁵ and are only briefly outlined here. The air intake of the Hg analyzer was located at the front of the vessel (approximately 15 m above the sea surface), opposite to the power system of the ship to minimize the impact of the smoke plume from the chimney. Sampling air was continuously pumped into the analyzer at a constant flow rate of 1 L·min⁻¹, and Hg was trapped on a gold cartridge and then thermally desorbed and detected by CVAES. Two soda lime tubes and a 0.45 μm PTFE filter were installed in front of the analyzer's inlet to prevent moisture and coarse particles (e.g., sea salt aerosols). The GEM measurements were calibrated daily using a built-in internal mercury permeation source within the analyzer. The detection limit (DL) for GEM measured by the 2537B unit was lower than 0.10 ng·m⁻³. DGM was measured based on the purging-trapping-detecting method adapted from Wang et al. (2017) and Fu et al. (2010).^{17,36} Approximately 1 L of the seawater sample was automatically poured from the seawater tap of the ship into a conditioned PTFE bubble chamber through a Teflon tube. As the DGM in the seawater with the similar volume could be purged to a concentration level close to 0 pg·L⁻³ in 60 min based on repeated trials, the water sample was purged with Hg-free air generated by a Tekran zero air generator at a flow rate of 1 L·min⁻¹ for 60 min. Meanwhile, the airstream was passed through a soda lime tube to remove moisture and was pumped by the Tekran 2537B for analysis. The detection limit is approximately 4.8 pg·L⁻¹.

2.3. Sea-Air Flux Calculation. The sea-air flux of Hg⁰ was calculated based on the thin-film gas exchange model.³⁷ In

general, the sea-air flux of Hg⁰ (F , ng·m⁻²·h⁻¹) was calculated using,

$$F = K_w(DGM - GEM/H'(T))$$

where K_w is the gas transfer velocity of elemental Hg in the air–water surface (cm·h⁻¹) and $H'(T)$ is Henry's Law constant. More details of this method can be found in Wang et al. (2017).¹⁷

2.4. Other Ancillary Data. Ozone (O₃) was continuously measured using a Thermo Fisher 49i ultraviolet photometer at a temporal resolution of 1 min. The DL of O₃ measurement was 1 part per billion by volume (ppbv). Hourly aerosol water-soluble Na⁺ were measured through a semicontinuous in situ gas and aerosol composition (IGAC) monitoring system.³⁸ Fine particles were enlarged through vapor condensation, accelerated via a conical-shaped impaction nozzle and collected on an impaction plate, and then measured Na⁺ and other ions by an online ion chromatography system (Dionex ICS-3000). The mass concentrations of black carbon (BC) were recorded every 30 min by a Model 5012 Multi-Angle Absorption Photometer (MAAP, Thermo Fisher Scientific Inc.).^{39,40} Sampling air flowed into the instrument at a rate of 1000 L·h⁻¹, and the particulate matter with particle size less than 2.5 μm (PM_{2.5}) were sampled on a glass filter tape (Schleicher and Schüll, type GF 10) under the detection of 670 nm light. Meteorological, hydrological, and GPS data were obtained from the ship's monitoring system, including true and apparent wind direction, wind speed (WS), air pressure (P), relative humidity (RH), atmospheric temperature (Temp), sea surface temperature (SST), surface seawater salinity, ship direction, and ship speed, all averaged over 5 min. Data on shortwave radiation (RD) were extracted from the assimilated hourly meteorological data from the GEOS-FP (horizontal resolution: 2° × 2.5°). In addition, some data were acquired from the NASA Global Modeling and Assimilation Office (GMAO) and Earth Observations (NEO) [e.g., the sulfur dioxide (SO₂) surface mass (https://fluid.nccs.nasa.gov/reanalysis/chem2d_merra2), precipitation (https://fluid.nccs.nasa.gov/reanalysis/classic_merra2), climatology, and wind speed anomalies (https://fluid.nccs.nasa.gov/reanalysis/anomaly_merra2)]. The HYSPLIT transport and dispersion model from NOAA-ARL (Air Resources Laboratory, <https://www.arl.noaa.gov/ready/hysplit4.html>) was used to identify the source of air masses from the selected points.⁴¹ Shortwave radiation (Radiation) data were extracted from the assimilated hourly meteorological data from GEOS-FP (horizontal resolution: 2° × 2.5°).

2.5. Simulation of GEM by the GEOS-Chem Model. The hourly concentrations of GEM were simulated using the GEOS-Chem global 3-D mercury model (v12.3.2) based on two different sets (see section 3.3.2). This model includes a global 3-D atmosphere (with a horizontal resolution of 2° × 2.5°, and 72 vertical layers in this study) and is coupled with the two-dimensional surface ocean and soil interfaces. The model is driven by assimilated meteorological data from the Goddard Earth Observation System (GEOS) of the NASA Global Modeling and Assimilation Office (GMAO), and it includes three separate tracers: Hg⁰, Hg^{II}, and Hg^P. The model couples a global anthropogenic Hg emission inventory [e.g., World Hg Emission Trends (WHET)], a global biomass burning Hg emission inventory [e.g., Global Fire Emissions Database (GFED-4)], and updated mechanisms for Hg redox chemistry.³⁴ The constant monthly oceanic evasion of Hg⁰ is

coupled in the GEOS-Chem model, which is outputted from the MITgcm model (Massachusetts Institute of Technology General Circulation Model).⁴² The model was run from 2016 to 2018 in the standard mode (which considers the emissions of anthropogenic and biomass burning sources), and was run from 2014 to 2018 in the mode that turned off the WHET anthropogenic mercury emission inventory and GFED-4 biomass burning mercury emission inventory (with two years of running time more than the standard mode, in order to eliminate the impact of anthropogenic emissions on atmospheric Hg latitudinal gradient in model), respectively. The simulated results of the 2018 was used in this study (section 3.3.2). More details of this model can be found in Zhang et al. (2019).²³

3. RESULTS AND DISCUSSION

3.1. General Characteristics of GEM in this Cruise. As shown in Figure 1a, the GEM concentrations of the oceanic area gradually increased from the southern hemisphere to the northern hemisphere, with an apparent latitudinal gradient. To further quantify the latitudinal differences in GEM observed during this cruise, we divided the observation field into three oceanic areas: southern Pacific (60°–20° S), tropical Pacific

(20° S–20° N), and northern Pacific (20°–30° N). The average GEM concentrations from the south to the north in these three areas were 0.86 ± 0.38 , 1.16 ± 0.46 , and 1.26 ± 0.23 ng·m⁻³, respectively (Table 1). Compared with the southern Pacific, the average GEM concentrations in the northern Pacific are increased by 0.4 ng·m⁻³. Similar differences in GEM concentrations between the hemispheres have also been observed in previous cruise observations.^{25,33} Higher GEM levels in the northern hemisphere reflect the impact of anthropogenic Hg emissions on the global cycle of atmospheric Hg. It is worth noting that the elevation in GEM average concentration from the southern Pacific to the tropical Pacific (34.9%) was significantly higher than that from the tropical Pacific to the northern Pacific (8.6%) during this cruise (*t* test, *p* < 0.001), despite the northern Pacific might be more impacted by higher anthropogenic emissions in the Northern Hemisphere. In addition, the standard deviation of GEM measurements in the tropical Pacific (0.46), which indicated the fluctuation amplitude of the GEM data, was also the largest among the three. This implies that some special mechanisms might intensify the latitudinal variation of GEM in the tropical oceanic area on a regional scale.

3.2. Accumulation of GEM in the Tropical Pacific.

Figure 1b shows the latitudinal series of the GEM during this cruise. Notably, an overall rise in GEM concentrations occurred from approximately 15°S to 10°N, where the GEM latitudinal gradient was the most apparent during this cruise (Figure 1a). As displayed in the light yellow shaded area of Figure 1b, the GEM concentrations showed an overall upward trend from 13°S to 2°S, with an increased amplitude of nearly 0.4 ng·m⁻³. Additionally, from the equator to 9° N, the GEM concentrations further increased by approximately 0.6 ng·m⁻³. The comparison between GEM and apparent wind direction (AWD) and black carbon (BC) data suggests that ship-based emissions were not the main cause of the increase in GEM (see Text S1 in the SI).

3.3. Potential Mechanisms of the GEM Accumulation in Tropical Pacific.

3.3.1. Potential Impact of the Doldrums. We further explored the relationships between GEM and other meteorological and chemical parameters, and found contrasting latitudinal tendencies between GEM and WS between 13°S and the equator (Figure 2a). A general elevation of GEM concentrations was accompanied by a continuous decrease in WS, with a significant negative linear correlation ($R^2 = 0.56$, $P < 0.01$, Figure 2b). From 13°S to the equator, the vessel will gradually approach the doldrums (the equatorial calm belt) in the western Pacific Ocean, which is also supported by the map of the monthly mean of WS in this area (Figure S3). As a weather system on a planetary scale, the low horizontal pressure gradient and windless weather in the doldrums would not be conducive to the dilution and transport of atmospheric pollutants. Our observations imply that the presence of the doldrums may be conducive to the accumulation of atmospheric GEM, which may delay its interhemispheric transport. In addition, it is noteworthy that the rising trend of GEM become more stable from about 8°S to 2°S than that in the southern area (15°S~8°S, Figures 2a and 3a). The negative correlations between the hourly GEM and WS in this two area were both significant, while with obviously higher correlation slope of hourly GEM vs WS from 8°S to 2°S (−0.016) than that in 15°S to 8°S (−0.046) (Figure S4), implying the facilitation of GEM accumulation by wind weakening may be affected by other factors in this area,

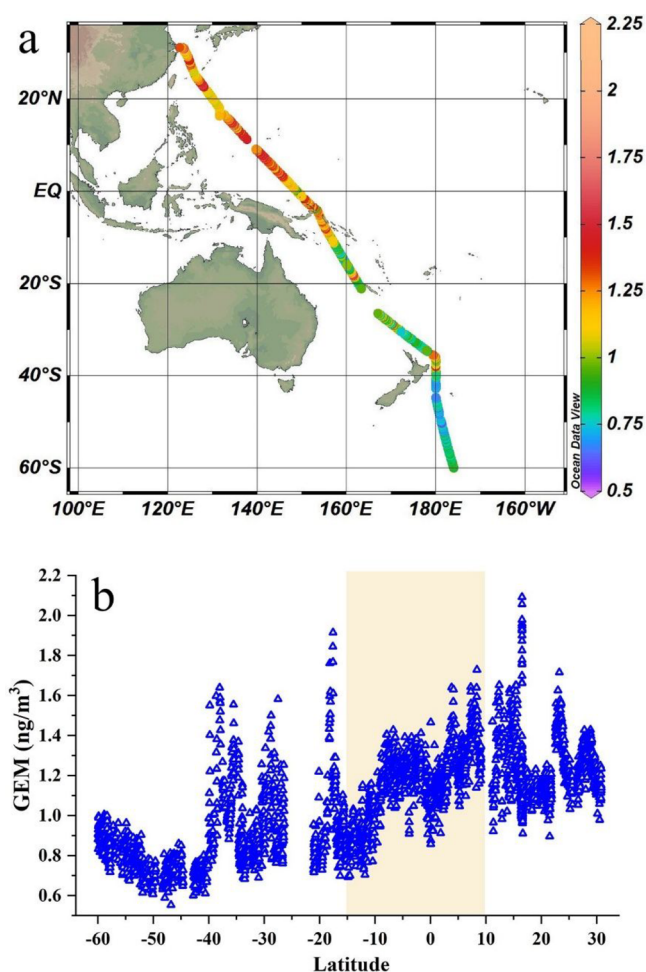


Figure 1. (a) The spatial distribution of gaseous elemental mercury (GEM) in this cruise observation, and (b) the latitudinal series of GEM concentration in this cruise observation. The light yellow shaded area shows the general rise of GEM concentrations occurred from ~15°S to ~10°N in the Tropical Pacific.

Table 1. Statistics for Gaseous Elemental Mercury (GEM) in the Three Oceanic Areas of This Cruise

areas	range (ng·m ⁻³)	average (ng·m ⁻³)	median (ng·m ⁻³)	no. of samples
Southern Pacific (60°S–20°S)	0.55–1.89	0.86 ± 0.38	0.84	1261
Tropical Pacific (20°S–20°N)	0.69–2.16	1.16 ± 0.46	1.16	1948
Northern Pacific (20°N–30°N)	0.90–1.77	1.26 ± 0.23	1.24	691

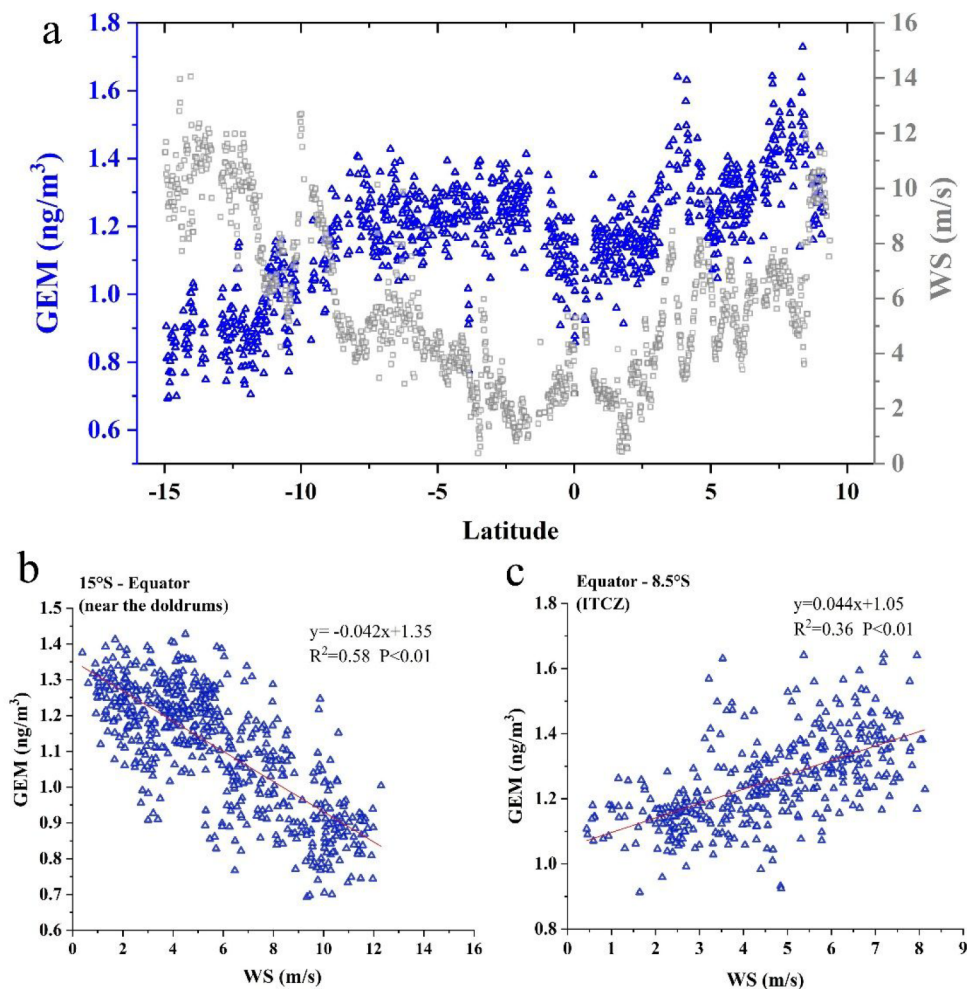


Figure 2. (a) The latitudinal series of GEM and wind speed (WS) in Tropical Pacific. (b) Linear correlation between GEM and WS in the cruise area of 15°S–Equator and (c) linear correlation between GEM and WS in the cruise area of Equator–8.5°N.

such as regional transport. To explore it, we compared the observed black carbon aerosol (BC) with GEM. As shown in Figure 3a, from 13°S to about 8°S, the rapid rising trend of GEM concentration was accompanied by the continuous increase of BC, with significant negative correlation between BC and WS ($r = -0.59$, $p < 0.01$), and its peak values are moderately beyond its background concentration in marine area ($50 \text{ ng}\cdot\text{m}^{-3}$),^{43,44} indicating the potential input from anthropogenic and/or geothermal sources; while from 8°S to about 2°S, the slower growth rate of GEM is along with the apparent decrease of BC concentrations (Figure 3a). These characteristics were in accordance with their meanwhile air mass sources: from 13°S to about 8°S, the air masses were frequently from the nearby islands, which may bring the inland contamination; while from 8°S to the equator, the air masses were mainly from the northwestern open sea (Figure 3b). Besides, the satellite data of surface SO₂ mass also showed the evidence of regional transport during the corresponding observation periods from 13°S to about 8°S (Figure S5).

This investigation suggests that the regional transport can further intensify the accumulation of GEM under the wind weakening condition when getting closer to the doldrums. The steadily rising trend of GEM without synchronize rise of BC near the doldrums (8°S~2°S) is likely to reflect the large differences in the residence time of GEM (from months up to 1 year) and BC (3.3~10.6 days) in the air,^{45,46} and further the different “accumulation effect” of doldrums on gaseous and particulate pollutants. Whether this potential “accumulation effect” is widely existed need further investigation.

In addition, atmospheric deposition of Hg mainly occurs in the form of oxidized phases (e.g., gaseous oxidized mercury or particle-bound mercury).^{29,47} Persistently low levels of O₃ (less than 10 ppbv) were observed from about 8°S to 2°S (Figure 4). The weak free-tropospheric input and photochemical dissociation of O₃ under poor NO_x conditions (an O₃ precursor) in the equatorial marine boundary layer result in a significant decrease in O₃ concentration.⁴⁸ In addition, as one of the most important sources of Br• radical, which is critical

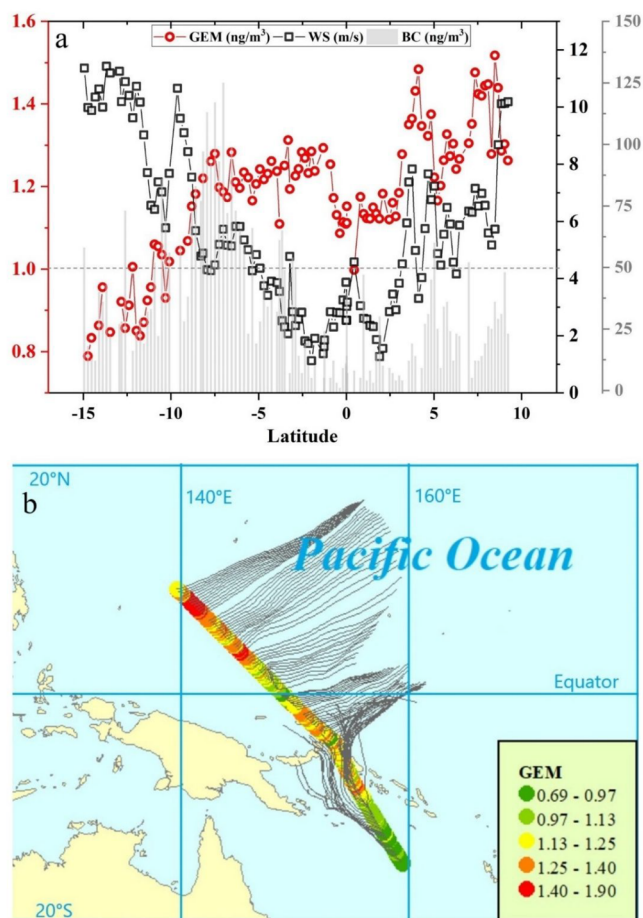
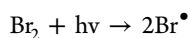
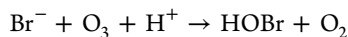


Figure 3. (a) The latitudinal series of hourly averaged GEM ($\text{ng}\cdot\text{m}^{-3}$), wind speed (WS), and black carbon in $\text{PM}_{2.5}$ (BC) in Tropical Pacific. The gray dash line indicates the background level of BC ($50 \text{ ng}\cdot\text{m}^{-3}$) in marine area. (b) The spatial distribution of gaseous elemental mercury (GEM), accompanied by the corresponding 72-h air mass backward trajectories during this cruise observation. Each backward trajectory was made every hour.

for the oxidation and subsequent deposition of Hg in the MBL, sea-salt aerosol is mainly generated by the wind-driven bubbles and wave-breaking processes.^{49,50} The calm weather in the doldrums is not conducive to the production of sea-salt aerosol, and it was supported by the corresponding high temporal-resolution measurements of aerosol Na^+ ions (a typical indicator of sea-salt aerosols in the MBL) in this cruise, which presents the persistently low levels of Na^+ (lower than $500 \text{ ng}\cdot\text{m}^{-3}$) from about 8°S to 2°S among the doldrums (Figure 4). The activation mechanisms of bromine on sea-salt aerosol can be demonstrated as follows:^{49,51}



The low concentrations of sea-salt aerosol and O_3 in the doldrums may not favor the activation of bromine in the MBL of this area, and it may be different from the upper troposphere which is rich in reactive halogen.^{52,53} Besides, the doldrums are dominated by the convergent updraft of the air mass, which may not be conducive to the input of reactive halogen components and/or Hg^{II} from the free troposphere. These

characteristics would lead to a weak oxidative environment for GEM in the boundary layer of this area. Previous observations in the CHARLEX campaign also found that the BrO^\bullet mixing ratio was always below the 2σ DL of 0.5 pptv in the tropical Pacific Ocean.⁵⁴ In addition, the high temperature of the equatorial area would not be conducive to the formation of HgBr^\bullet due to the pyrolysis effect. As a result, the weak potential oxidative capacity of the MBL in the doldrums might intensify the accumulation of GEM in the tropical Pacific.

3.3.2. Potential Impact of the Intertropical Convergence Zone. Interestingly, unlike the area from 13°S to the equator, GEM presented a similar latitudinal pattern with WS from the equator to about 8.5°N , with a significant positive linear correlation ($R^2 = 0.36$, $P < 0.01$, Figure 2b). It should be explored whether this positive correlation between GEM and WS indicated the impact of atmospheric transport from anthropogenic and/or volcanic sources on the GEM elevation in this area. First, the backward trajectory analysis presents that the corresponding air masses during this cruise (from the equator to about 10°N) were mainly from the northeastern oceanic area. Second, the observed BC concentrations during this cruise were mainly below its background level in marine area ($50 \text{ ng}\cdot\text{m}^{-3}$).^{43,44} Third, the comparison between observations and GEOS-Chem simulations of GEM presented that the simulated results could not capture the increasing trend of GEM concentrations and its corresponding high values from about 5°N to 8.5°N , despite the simulation has considered the emissions of anthropogenic and biomass burning sources (in the standard mode) (Figure S6). Besides, after removing the impacts of anthropogenic and biomass burning sources (turning off the WHET anthropogenic mercury emission inventory and GFED-4 biomass burning mercury emission inventory), the simulated results could still generally capture the overall rising trend of GEM from the equator to about 3°N (Figure S6). These characteristics all indicated that the upward latitudinal trend of GEM in this area should not be attributed only to the anthropogenic, biomass burning, and/or volcanic contributions in the Northern hemisphere.

It is worth noting that this area is located in the ITCZ, which is characterized by high temperatures and frequent convective precipitation.⁵⁵ Horowitz et al. (2017)⁵⁶ indicated that 80% of the global wet deposition of Hg occurs over the oceanic areas, with a major proportion occurring in the tropics, based on their modeling studies. Previous observations have shown that abundant wet deposition of Hg and its corresponding strong photoreduction in the ITCZ can lead to a significant increase in the concentration of Hg^0 in the surface seawater (Kuss et al., 2011; Soerensen et al., 2014). Evasion also substantially contributes to atmospheric Hg^0 over the marine boundary layer, especially in the open sea area.^{2,57} The corresponding backward trajectory during the continuous cruise observation in this area showed that the air masses were mainly transported near the sea surface (Figure 3b), implying that the higher release of Hg^0 from surface seawater promoted by the increase in WS is likely to be a potential driving factor that cause the increase of atmospheric GEM concentrations in this area.

To further explore these mechanisms, we investigated the relationships between the DGM, Hg air-sea flux, and GEM, and found that similar to GEM, the measured concentrations of DGM were also generally higher in the north of the equator than in the southern area (Figure 5). The highest DGM levels

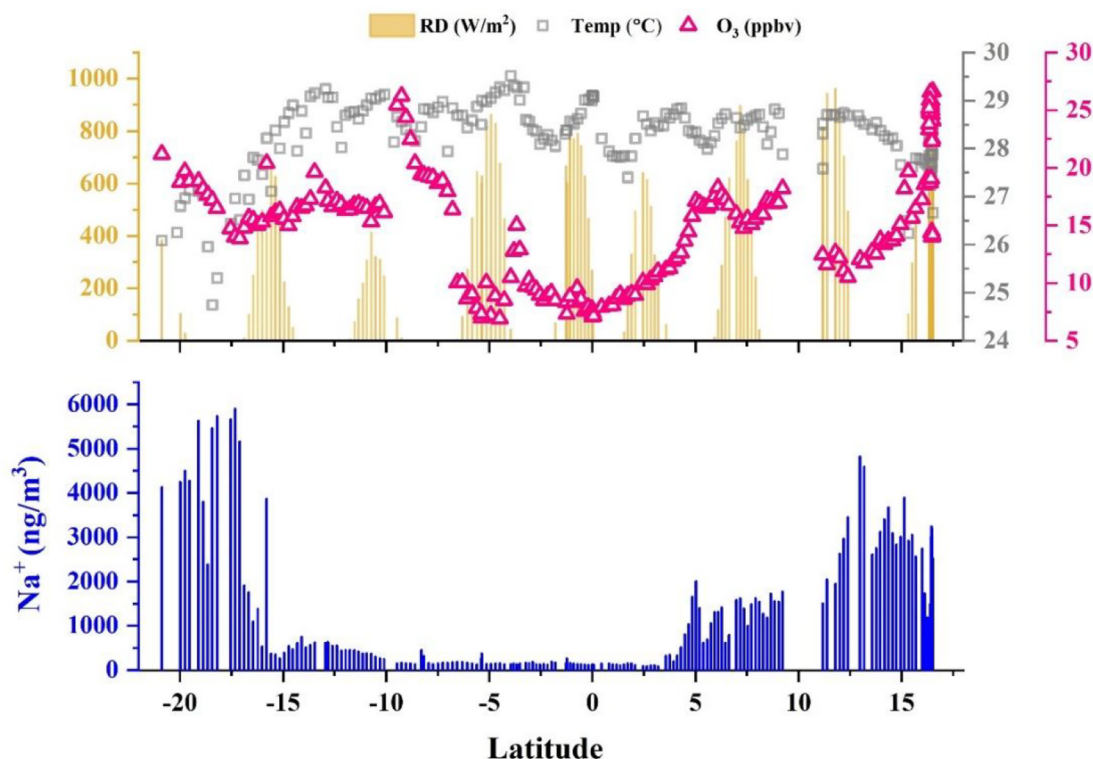


Figure 4. Latitudinal series of measured hourly aerosol Na^+ ion and O_3 concentrations, and meteorological parameters (include temperature (Temp) and shortwave radiation (RD)) in the Tropical Pacific.

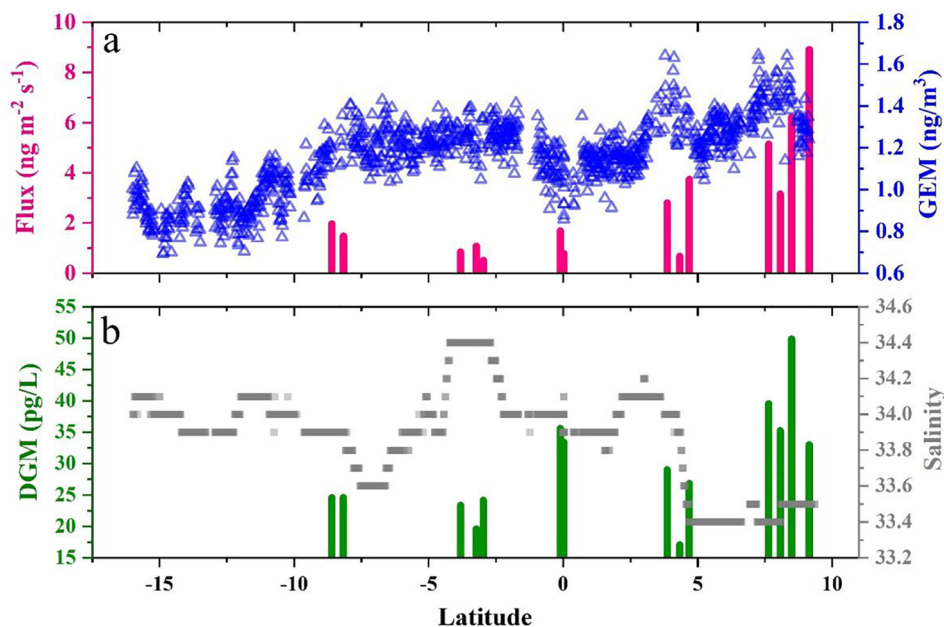


Figure 5. Latitudinal series of GEM, dissolved gaseous mercury (DGM), calculated Hg sea-air flux and salinity of surface seawater in the cruise area of $-15^{\circ}\text{S}\sim 10^{\circ}\text{N}$.

($\sim 50 \text{ pg}\cdot\text{L}^{-1}$) were measured at approximately 8°N , accompanied by apparently decreases in surface seawater salinity, implying the potential role of wet deposition of Hg on the elevation of DGM and the dilution of seawater. The MERRA-2 precipitation map also displays an intense precipitation belt between the equator and 10°N in the western Pacific, 1–2 days prior to our cruise observation period (Figure S7). Driven by the Walker Circulation,⁵⁸ the

western side of the equatorial Pacific is wet with frequent rainfall due to the collected moisture and convective updraft. Furthermore, from the equator to 9°N , the sea-air flux of Hg presents a similar rising latitudinal tendency as that of GEM, which was driven by the increase of DGM and WS, with the peak flux of $8.91 \text{ ng}\cdot\text{m}^{-3}\cdot\text{h}^{-1}$ at approximately 9°N (Figure 5). The average sea-air flux of Hg in the north of the equator ($3.93 \pm 2.77 \text{ ng}\cdot\text{m}^{-3}\cdot\text{h}^{-1}$), which is similar to the level observed in

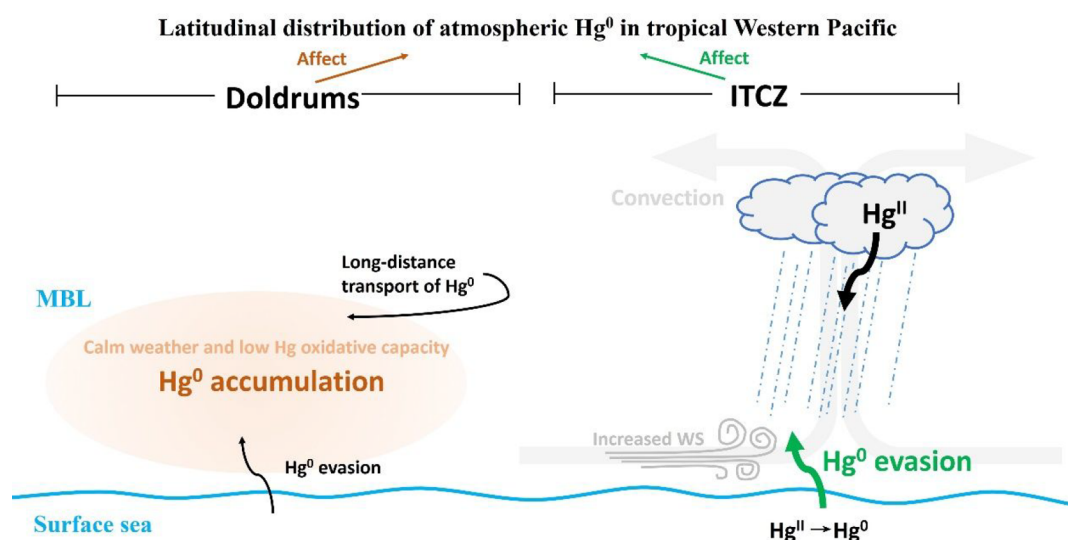


Figure 6. A schematic diagram simply displays the potential mechanisms that impact the latitudinal distribution of GEM (Hg^0) in the tropical western Pacific by the doldrums and the Inter-Tropical Conversion Zone (ITCZ) in this area, which are discussed in this study. For the doldrums, calm weather may delay the transport of GEM, leading to its accumulation in the tropical western Pacific. Furthermore, the regional transport, and the low O_3 and sea-salt aerosol levels which would be not conducive to the oxidation of GEM in the boundary layer in this area, which may further intensify the accumulation of GEM in the tropical western Pacific. For the ITCZ, the vast wet deposition of Hg would drive elevated DGM in the surface seawater, which can increase the sea-air flux and may further influence the spatial distribution of GEM.

the ITCZ in Soerensen et al. (2014),¹³ is nearly thrice that in the southern area ($1.27 \pm 0.55 \text{ ng}\cdot\text{m}^{-3}\cdot\text{h}^{-1}$). These features further imply the potential role of wet deposition, photo-reduction and the subsequent sea-air exchange of Hg in the spatial distribution of GEM in the ITCZ. In all, the potential mechanisms that impact the latitudinal distribution of GEM (Hg^0) in the tropical western Pacific by the doldrums and the Inter-Tropical Conversion Zone (ITCZ) in this area, which are discussed in this study, was simply illustrating in a schematic diagram in Figure 6.

■ ASSOCIATED CONTENT

SI Supporting Information

The Supporting Information is available free of charge at <https://pubs.acs.org/doi/10.1021/acs.est.1c07229>.

Evaluation of the influence of ship emissions; tracks of the cruises in this study; correlations between hourly GEM and WS; spatial distributions of monthly statistics of wind speed, surface SO_2 , and 24-h accumulated precipitation; and comparison between observations and GEOS-Chem simulations of GEM in two different modes (PDF)

■ AUTHOR INFORMATION

Corresponding Author

Zhouqing Xie – Institute of Polar Environment & Anhui Key Laboratory of Polar Environment and Global Change, Department of Environmental Science and Engineering, University of Science and Technology of China, Hefei, Anhui 230026, P. R. China; Center for Excellence in Urban Atmospheric Environment, Institute of Urban Environment, Chinese Academy of Sciences, Xiamen, Fujian 361021, P. R. China; orcid.org/0000-0003-1703-5157; Email: zqxie@ustc.edu.cn

Authors

Fange Yue – Institute of Polar Environment & Anhui Key Laboratory of Polar Environment and Global Change, Department of Environmental Science and Engineering, University of Science and Technology of China, Hefei, Anhui 230026, P. R. China

Yanxu Zhang – School of Atmospheric Sciences, Nanjing University, Nanjing 210023, P. R. China

Jinpei Yan – Key Laboratory of Global Change and Marine-Atmospheric Chemistry, Third Institute of Oceanography, Ministry of Natural Resources, Xiamen 361005, P. R. China; orcid.org/0000-0002-1273-9422

Shuhui Zhao – Key Laboratory of Global Change and Marine-Atmospheric Chemistry, Third Institute of Oceanography, Ministry of Natural Resources, Xiamen 361005, P. R. China

Complete contact information is available at: <https://pubs.acs.org/doi/10.1021/acs.est.1c07229>

Notes

The authors declare no competing financial interest.

■ ACKNOWLEDGMENTS

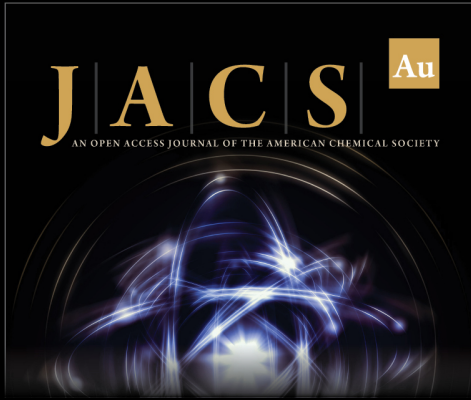
This work was supported by the National Natural Science Foundation of China (grant no. 41941014, 41930532), and Ministry of Natural Resources of the People's Republic of China (IRASCC2020-2022-No.01-01-02E). We thank China Arctic and Antarctic Administration for fieldwork support. The authors acknowledge the NOAA Air Resources Laboratory (ARL) for developing the HYSPLIT transport and dispersion model available on the Internet (<https://www.ready.noaa.gov/HYSPLIT.php>).

■ REFERENCES

- (1) Mason, R. P.; Sheu, G. R. Role of the ocean in the global mercury cycle. *Global Biogeochemical Cycles* **2002**, *16* (4), 40-1–40-14.


- (2) Strode, S. A.; Jaeglé, L.; Selin, N. E.; Jacob, D. J.; Park, R. J.; Yantosca, R. M.; Mason, R. P.; Slemr, F. Air-sea exchange in the global mercury cycle. *Global Biogeochemical Cycles* **2007**, *21* (1), GB10171-12.
- (3) Holmes, C. D.; Jacob, D. J.; Corbitt, E. S.; Mao, J.; Yang, X.; Talbot, R.; Slemr, F. Global atmospheric model for mercury including oxidation by bromine atoms. *Atmospheric Chemistry and Physics* **2010**, *10* (24), 12037–12057.
- (4) Sunderland, E. M.; Mason, R. P. Human impacts on open ocean mercury concentrations. *Global Biogeochemical Cycles* **2007**, *21* (4), GB40221-15.
- (5) Nerentorp Mastromonaco, M.; Gårdfeldt, K.; Jourdain, B.; Abrahamsson, K.; Granfors, A.; Ahnoff, M.; Dommergue, A.; Méjean, G.; Jacobi, H. W. Antarctic winter mercury and ozone depletion events over sea ice. *Atmos. Environ.* **2016**, *129*, 125–132.
- (6) Driscoll, C. T.; Mason, R. P.; Chan, H. M.; Jacob, D. J.; Pirrone, N. Mercury as a global pollutant: sources, pathways, and effects. *Environ. Sci. Technol.* **2013**, *47* (10), 4967–4983.
- (7) Andersson, M. E.; Sommar, J.; Gårdfeldt, K.; Lindqvist, O. Enhanced concentrations of dissolved gaseous mercury in the surface waters of the Arctic Ocean. *Marine Chemistry* **2008**, *110* (3), 190–194.
- (8) Kim, J. P.; Fitzgerald, W. F. Sea-air partitioning of mercury in the equatorial Pacific Ocean. *Science* **1986**, *231* (4742), 1131–1133.
- (9) Andersson, M. E.; Sommar, J.; Gårdfeldt, K.; Jutterström, S. Air-sea exchange of volatile mercury in the North Atlantic Ocean. *Marine Chemistry* **2011**, *125* (1), 1–7.
- (10) Kuss, J.; Züllicke, C.; Pohl, C.; Schneider, B. Atlantic mercury emission determined from continuous analysis of the elemental mercury sea-air concentration difference within transects between 50°N and 50°S. *Global Biogeochemical Cycles* **2011**, *25* (3), GB30211-9.
- (11) Ci, Z. J.; Zhang, X. S.; Wang, Z. W.; Niu, Z. C.; Diao, X. Y.; Wang, S. W. Distribution and air-sea exchange of mercury (Hg) in the Yellow Sea. *Atmospheric Chemistry and Physics* **2011**, *11* (6), 2881–2892.
- (12) Fu, X.; Feng, X.; Zhang, G.; Xu, W.; Li, X.; Yao, H.; Liang, P.; Li, J.; Sommar, J.; Yin, R.; Liu, N. Mercury in the marine boundary layer and seawater of the South China Sea: Concentrations, sea/air flux, and implication for land outflow. *Journal of Geophysical Research* **2010**, *115* (D6), D063031-11.
- (13) Soerensen, A. L.; Mason, R. P.; Balcom, P. H.; Jacob, D. J.; Zhang, Y.; Kuss, J.; Sunderland, E. M. Elemental mercury concentrations and fluxes in the tropical atmosphere and ocean. *Environ. Sci. Technol.* **2014**, *48* (19), 11312–11319.
- (14) Kuss, J.; Wasmund, N.; Nausch, G. n.; Labrenz, M. Mercury Emission by the Baltic Sea: A consequence of cyanobacterial activity, photochemistry, and low-light mercury Transformation. *Environ. Sci. Technol.* **2015**, *49* (19), 11449–11457.
- (15) Ci, Z.; Zhang, X.; Wang, Z. Air-sea exchange of gaseous mercury in the tropical coast (Luhuitou fringing reef) of the South China Sea, the Hainan Island. *China. Environmental Science and Pollution Research* **2016**, *23*, 11323.
- (16) Kuss, J.; Krüger, S.; Ruickoldt, J.; Wlost, K. P. High-resolution measurements of elemental mercury in surface water for an improved quantitative understanding of the Baltic Sea as a source of atmospheric mercury. *Atmos. Chem. Phys. Discuss.* **2018**, *18*, 4361.
- (17) Wang, J.; Xie, Z.; Wang, F.; Kang, H. Gaseous elemental mercury in the marine boundary layer and air-sea flux in the Southern Ocean in austral summer. *Science of The Total Environment* **2017**, *603–604*, 510–518.
- (18) Bagnato, E.; Sproveri, M.; Barra, M.; Bitetto, M.; Bonsignore, M.; Calabrese, S.; Di Stefano, V.; Oliveri, E.; Parello, F.; Mazzola, S. The sea-air exchange of mercury (Hg) in the marine boundary layer of the Augusta basin (southern Italy): Concentrations and evasion flux. *Chemosphere* **2013**, *93* (9), 2024–2032.
- (19) Gårdfeldt, K.; Sommar, J.; Ferrara, R.; Ceccarini, C.; Lanzillotta, E.; Munthe, J.; Wangberg, I.; Lindqvist, O.; Pirrone, N.; Sprovieri, F.; Pesenti, E.; Stromberg, D. Evasion of mercury from coastal and open waters of the Atlantic Ocean and the Mediterranean Sea. *Atmos. Environ.* **2003**, *37*, 73–84.
- (20) Wängberg, I.; Schmolke, S.; Schager, P.; Munthe, J.; Ebinghaus, R.; Iverfeldt, A. Estimates of air-sea exchange of mercury in the Baltic Sea. *Atmos. Environ.* **2001**, *35* (32), 5477–5484.
- (21) Pirrone, N.; Mason, R. *Mercury Fate and Transport in the Global Atmosphere*; Springer Science & Business Media: New York, 2009, pp 173–191.
- (22) Travníkov, O. Atmospheric transport of mercury. *Environmental Chemistry and Toxicology of Mercury* **2011**, 329–365.
- (23) Zhang, Y.; Horowitz, H.; Wang, J.; Xie, Z.; Kuss, J.; Soerensen, A. L. A Coupled Global Atmosphere-Ocean Model for Air-Sea Exchange of Mercury: Insights into Wet Deposition and Atmospheric Redox Chemistry. *Environ. Sci. Technol.* **2019**, *53* (9), 5052–5061.
- (24) Liu, Y.; Guo, L.; Wu, G.; Wang, Z. Sensitivity of ITCZ configuration to cumulus convective parameterizations on an aqua planet. *Climate Dynamics* **2010**, *34* (2), 223–240.
- (25) Seiler, W.; Eberling, C.; Slemr, F. Global distribution of gaseous mercury in the troposphere. *pure and applied geophysics* **1980**, *118* (2), 964–974.
- (26) Slemr, F.; Junkermann, W.; Schmidt, R.; Sladkovic, R. Indication of change in global and regional trends of atmospheric mercury concentrations. *Geophys. Res. Lett.* **1995**, *22* (16), 2143–2146.
- (27) Slemr, F.; Schuster, G.; Seiler, W. Distribution, speciation, and budget of atmospheric mercury. *Journal of atmospheric chemistry* **1985**, *3* (4), 407–434.
- (28) Slemr, F.; Seiler, W.; Schuster, G. Latitudinal distribution of mercury over the Atlantic Ocean. *Journal of Geophysical Research: Oceans* **1981**, *86* (C2), 1159–1166.
- (29) Soerensen, A. L.; Skov, H.; Jacob, D. J.; Soerensen, B. T.; Johnson, M. S. Global Concentrations of Gaseous Elemental Mercury and Reactive Gaseous Mercury in the Marine Boundary Layer. *Environ. Sci. Technol.* **2010**, *44* (19), 7425–7430.
- (30) Slemr, F.; Langer, E. Increase in global atmospheric concentrations of mercury inferred from measurements over the Atlantic Ocean. *Nature* **1992**, *355*, 434–437.
- (31) Temme, C.; Slemr, F.; Ebinghaus, R.; Einax, J. Distribution of mercury over the Atlantic Ocean in 1996 and 1999–2001. *Atmos. Environ.* **2003**, *37* (14), 1889–1897.
- (32) Müller, D.; Wip, D.; Warneke, T.; Holmes, C.; Dastoor, A.; Notholt, J. Sources of atmospheric mercury in the tropics: continuous observations at a coastal site in Suriname. *Atmospheric Chemistry and Physics* **2012**, *12* (16), 7391–7397.
- (33) Xia, C.; Xie, Z.; Sun, L. Atmospheric mercury in the marine boundary layer along a cruise path from Shanghai, China to Prydz Bay, Antarctica. *Atmos. Environ.* **2010**, *44* (14), 1815–1821.
- (34) Horowitz, H. M.; Jacob, D. J.; Zhang, Y.; Dibble, T. S.; Slemr, F.; Amos, H. M.; Schmidt, J. A.; Corbitt, E. S.; Marais, E. A.; Sunderland, E. M. A new mechanism for atmospheric mercury redox chemistry: implications for the global mercury budget. *Atmospheric Chemistry and Physics* **2017**, *17* (10), 6353–6371.
- (35) Yu, J.; Xie, Z.; Kang, H.; Li, Z.; Sun, C.; Bian, L.; Zhang, P. High variability of atmospheric mercury in the summertime boundary layer through the central Arctic Ocean. *Sci. Rep.* **2015**, *4* (1), 6091.
- (36) Fu, X.; Feng, X.; Zhang, G.; Xu, W.; Li, X.; Yao, H.; Liang, P.; Li, J.; Sommar, J.; Yin, R.; Liu, N. Mercury in the marine boundary layer and seawater of the South China Sea: Concentrations, sea/air flux, and implication for land outflow. *J. Geophys. Res.: Atmos.* **2010**, *115*, (D6) DOI: 10.1029/2009JD012958.
- (37) Wanninkhof, R. Relationship between wind speed and gas exchange over the ocean. *Journal of Geophysical Research: Oceans* **1992**, *97* (C5), 7373–7382.
- (38) Yan, J.; Jung, J.; Zhang, M.; Bianchi, F.; Tham, Y. J.; Xu, S.; Lin, Q.; Zhao, S.; Li, L.; Chen, L. Uptake selectivity of methanesulfonic acid (MSA) on fine particles over polynya regions of the Ross Sea, Antarctica. *Atmospheric Chemistry and Physics* **2020**, *20* (5), 3259–3271.


- (39) Petzold, A.; Feldpausch, P.; Fritzsche, L.; Minikin, A.; Lauer, P.; Bauer, H. PARTICLE EMISSIONS FROM SHIP ENGINES. *J. Aerosol Sci.* **2004**, *35*, S1095–S1096.
- (40) Petzold, A.; Schloesser, H.; Sheridan, P. J.; Arnott, W. P.; Ogren, J. A.; Virkkula, A. Evaluation of Multiangle Absorption Photometry for Measuring Aerosol Light Absorption. *Aerosol Sci. Technol.* **2005**, *39* (1), 40–51.
- (41) Wang, Y. Q.; Zhang, X. Y.; Draxler, R. R. TrajStat: GIS-based software that uses various trajectory statistical analysis methods to identify potential sources from long-term air pollution measurement data. *Environmental Modelling & Software* **2009**, *24* (8), 938–939.
- (42) Huang, S.; Zhang, Y. Interannual Variability of Air–Sea Exchange of Mercury in the Global Ocean: The “Seesaw Effect” in the Equatorial Pacific and Contributions to the Atmosphere. *Environ. Sci. Technol.* **2021**, *55* (10), 7145–7156.
- (43) Moorthy, K. K.; Satheesh, S. K.; Babu, S. S.; Saha, A. Large latitudinal gradients and temporal heterogeneity in aerosol black carbon and its mass mixing ratio over southern and northern oceans observed during a trans-continental cruise experiment. *Geophys. Res. Lett.* **2005**, *32* (14), L148181–4.
- (44) Samset, B. H.; Myhre, G.; Herber, A.; Kondo, Y.; Li, S. M.; Moteki, N.; Koike, M.; Oshima, N.; Schwarz, J. P.; Balkanski, Y.; Bauer, S. E.; Bellouin, N.; Bernsten, T. K.; Bian, H.; Chin, M.; Diehl, T.; Easter, R. C.; Ghan, S. J.; Iversen, T.; Kirkevåg, A.; Lamarque, J. F.; Lin, G.; Liu, X.; Penner, J. E.; Schulz, M.; Seland, Ø.; Skeie, R. B.; Stier, P.; Takemura, T.; Tsigaridis, K.; Zhang, K. Modelled black carbon radiative forcing and atmospheric lifetime in AeroCom Phase II constrained by aircraft observations. *Atmospheric Chemistry and Physics* **2014**, *14* (22), 12465–12477.
- (45) Bond, T. C.; Doherty, S. J.; Fahey, D. W.; Forster, P. M.; Bernsten, T.; DeAngelo, B. J.; Flanner, M. G.; Ghan, S.; Kärcher, B.; Koch, D.; Kinne, S.; Kondo, Y.; Quinn, P. K.; Sarofim, M. C.; Schultz, M. G.; Schulz, M.; Venkataraman, C.; Zhang, H.; Zhang, S.; Bellouin, N.; Guttikunda, S. K.; Hopke, P. K.; Jacobson, M. Z.; Kaiser, J. W.; Klimont, Z.; Lohmann, U.; Schwarz, J. P.; Shindell, D.; Storelvmo, T.; Warren, S. G.; Zender, C. S. Bounding the role of black carbon in the climate system: A scientific assessment. *Journal of Geophysical Research: Atmospheres* **2013**, *118* (11), 5380–5552.
- (46) Yue, F.; Xie, Z.; Yan, J.; Zhang, Y.; Jiang, B. Spatial Distribution of Atmospheric Mercury Species in the Southern Ocean. *Journal of Geophysical Research: Atmospheres* **2021**, *126* (17), No. e2021JD034651.
- (47) Lindberg, S.; Bullock, R.; Ebinghaus, R.; Engstrom, D.; Feng, X.; Fitzgerald, W.; Pirrone, N.; Prestbo, E.; Seigneur, C. A Synthesis of Progress and Uncertainties in Attributing the Sources of Mercury in Deposition. *AMBIO: A Journal of the Human Environment* **2007**, *36* (1), 19–33.
- (48) Singh, H. B.; Herlth, D.; Kolyer, R.; Salas, L.; Bradshaw, J. D.; Sandholm, S. T.; Davis, D. D.; Crawford, J.; Kondo, Y.; Koike, M.; Talbot, R.; Gregory, G. L.; Sachse, G. W.; Browell, E.; Blake, D. R.; Rowland, F. S.; Newell, R.; Merrill, J.; Heikes, B.; Liu, S. C.; Crutzen, P. J.; Kanakidou, M. Reactive nitrogen and ozone over the western Pacific: Distribution, partitioning, and sources. *Journal of Geophysical Research: Atmospheres* **1996**, *101* (D1), 1793–1808.
- (49) Zhu, L.; Jacob, D. J.; Eastham, S. D.; Sulprizio, M. P.; Wang, X.; Sherwen, T.; Evans, M. J.; Chen, Q.; Alexander, B.; Koenig, T. K.; Volkamer, R.; Huey, L. G.; Le Breton, M.; Bannan, T. J.; Percival, C. J. Effect of sea salt aerosol on tropospheric bromine chemistry. *Atmospheric Chemistry and Physics* **2019**, *19* (9), 6497–6507.
- (50) Luo, Y.; Si, F.; Zhou, H.; Dou, K.; Liu, Y.; Liu, W. Observations and source investigations of the boundary layer bromine monoxide (BrO) in the Ny-Ålesund Arctic. *Atmospheric Chemistry and Physics* **2018**, *18* (13), 9789–9801.
- (51) Hara, K.; Osada, K.; Yabuki, M.; Takashima, H.; Theys, N.; Yamanouchi, T. Important contributions of sea-salt aerosols to atmospheric bromine cycle in the Antarctic coasts. *Sci. Rep.* **2018**, *8* (1), 13852.
- (52) Schmidt, J. A.; Jacob, D. J.; Horowitz, H. M.; Hu, L.; Sherwen, T.; Evans, M. J.; Liang, Q.; Suleiman, R. M.; Oram, D. E.; Le Breton, M.; Percival, C. J.; Wang, S.; Dix, B.; Volkamer, R. Modeling the observed tropospheric BrO background: Importance of multiphase chemistry and implications for ozone, OH, and mercury. *Journal of Geophysical Research: Atmospheres* **2016**, *121* (19), 11819–11835.
- (53) Gratz, L. E.; Ambrose, J. L.; Jaffe, D. A.; Shah, V.; Jaeglé, L.; Stutz, J.; Festa, J.; Spolaor, M.; Tsai, C.; Selin, N. E.; Song, S.; Zhou, X.; Weinheimer, A. J.; Knapp, D. J.; Montzka, D. D.; Flocke, F. M.; Campos, T. L.; Apel, E.; Hornbrook, R.; Blake, N. J.; Hall, S.; Tyndall, G. S.; Reeves, M.; Stechman, D.; Stell, M. Oxidation of mercury by bromine in the subtropical Pacific free troposphere. *Geophys. Res. Lett.* **2015**, *42* (23), 10494–10502.
- (54) Wang, F.; Saiz-Lopez, A.; Mahajan, A. S.; Gómez Martín, J. C.; Armstrong, D.; Lemes, M.; Hay, T.; Prados-Roman, C. Enhanced production of oxidised mercury over the tropical Pacific Ocean: a key missing oxidation pathway. *Atmospheric Chemistry and Physics* **2014**, *14* (3), 1323–1335.
- (55) Byrne, M. P.; Schneider, T. Narrowing of the ITCZ in a warming climate: Physical mechanisms. *Geophys. Res. Lett.* **2016**, *43* (21), 11350–11357.
- (56) Horowitz, H. M.; Jacob, D. J.; Zhang, Y.; Dibble, T. S.; Slemr, F.; Amos, H. M.; Schmidt, J. A.; Corbitt, E. S.; Marais, E. A.; Sunderland, E. M. A new mechanism for atmospheric mercury redox chemistry: implications for the global mercury budget. *Atmospheric Chemistry and Physics* **2017**, *17* (10), 6353–6371.
- (57) Mason, R. P.; Hammerschmidt, C. R.; Lamborg, C. H.; Bowman, K. L.; Swarr, G. J.; Shelley, R. U. The air-sea exchange of mercury in the low latitude Pacific and Atlantic Oceans. *Deep Sea Research Part I: Oceanographic Research Papers* **2017**, *122*, 17–28.
- (58) Wikipedia, Walker circulation. https://en.wikipedia.org/wiki/Walker_circulation, 2017 (The page was last edited on 21 August 2017).



JACS Au
AN OPEN ACCESS JOURNAL OF THE AMERICAN CHEMICAL SOCIETY

Editor-in-Chief
Prof. Christopher W. Jones
Georgia Institute of Technology, USA

Open for Submissions 

pubs.acs.org/jacsau  ACS Publications
Most Trusted. Most Cited. Most Read.